J Mol Model (2011) 17:2395–2409
DOI 10.1007/s00894-011-0988-5

ORIGINAL PAPER

Mechanism of the gas-phase decomposition of trifluoro-, trichloro-, and tribromomethanols in the presence of hydrogen halides

Katarzyna Brudnik · Jerzy T. Jodkowski · Dariusz Sarzyński · Andrzej Nowek

Received: 11 October 2010 / Accepted: 24 January 2011 / Published online: 2 March 2011

Abstract *Ab initio* calculations at the G2 level were used in a theoretical analysis of the kinetics of the decomposition of trifluoro-, trichloro-, and tribromomethanols. The high-pressure limiting rate coefficients $k_{diss,\infty}$ for the thermal dissociation of CF_3OH, CCl_3OH, and CBr_3OH were calculated using the conventional transition state theory. The results of potential surface calculations show that in the presence of the hydrogen halides HX (X = F, Cl, and Br), considerably lower energy pathways are accessible for the decomposition of CF_3OH, CCl_3OH, and CBr_3OH. The mechanism of the reactions appears to be complex and consists of three consecutive elementary processes with the formation of pre- and post-reaction adducts. The presence of hydrogen halides considerably decreases the energy barrier for the bimolecular decomposition of the alcohols CF_3OH, CCl_3OH, and CBr_3OH. Results of this study indicate that hydrogen halides can considerably accelerate the homogeneous decomposition of perhalogenated methanols when they are present in the reaction area at sufficiently high concentrations. However, the atmospheric concentrations of hydrogen halides are too small for efficient removal of atmospheric CF_3OH, CCl_3OH, and CBr_3OH.

Keywords Gas-phase kinetics · Tribromometanol · Trichloromethanol · Trifluoromethanol

K. Brudnik · J. T. Jodkowski (✉) · D. Sarzyński · A. Nowek
Department of Physical Chemistry, Wroclaw Medical University,
pl. Nankiera 1,
50-140, Wroclaw, Poland
e-mail: jurek@kchfiz.am.wroc.pl

Introduction

The perhalogenated alcohols trifluoro-, trichloro-, and tribromomethanol occur in the atmosphere as products of the photofragmentation of alternative halocarbons [1, 2]. They take part in many degradation processes in the atmosphere and in various combustion systems [2]. In the oxygen-rich atmosphere, the primary atmospheric fate of alkyl radicals is the addition reaction with molecular oxygen. The halogenated methyl radicals CF_3, CCl_3, and CBr_3 are converted into the corresponding methylperoxy structures CY_3O_2 (Y = F, Cl, and Br), which then react with nitric oxide, generating trifluoro-, trichloro-, and tribromomethoxy CY_3O radicals [1, 3]. The subsequent fate of the CY_3O radicals is considerably less known. However, results of kinetic studies suggest that the loss of CY_3O radicals in the lower atmosphere is mainly related to reactions with nitrogen oxides. Alternative pathways, i.e., reactions between CY_3O, H_2O, and hydrogen halides (HX) or hydrocarbons (RH), lead to the formation of the respective perhalogenated alcohols:

$$CY_3O + (H_2O, HX, RH) \rightarrow CY_3OH + (OH, X, R) \qquad (1)$$

where X, Y = F, Cl, and Br. The formed CY_3OH alcohols may act as temporary halogen reservoir species. The subsequent reactions of CY_3OH molecule leading to its removal from the atmosphere are thus important for a better understanding of the possible processes of CY_3O loss. Therefore the kinetics and mechanism of the decomposition of the perhalogenated alcohols have become the subject of several experimental and theoretical investigations [4–29].

Trifluoromethanol CF_3OH has been the most frequently studied. Results of theoretical studies [11–29] show that the CF_3O-H bond is unusually strong, which can be attributed

to the negative hyperconjugative effect of the CF_3 group. This implies high activation energy values for hydrogen abstraction from CF_3OH, which has been confirmed by experimental investigations [4–7]. The photolysis of CF_3OH has also been shown to be inefficient [5, 6]. The thermal decomposition of trifluoromethanol with the elimination of hydrogen fluoride

$$CF_3OH \rightarrow COF_2 + HF \quad (2)$$

was studied theoretically[11, 13–15, 29] and experimentally [4–8]. The energy barrier calculated at various levels of theory is high (150-170 kJ mol^{-1}), which results in a very small reaction rate at ambient temperature. However, there is some experimental evidence strongly suggesting that atmospheric CF_3OH can be efficiently decomposed heterogeneously on H_2O surfaces [10]. Theoretical investigations show that water can introduce many unusual features into the kinetics and energetics of some chemical reaction systems [10, 30–32]. *Ab initio* calculations indicate unambiguously that the decomposition of CF_3OH on water aerosols seems to be a major process in the loss of atmospheric CF_3OH [10, 14, 15].

The kinetics of the thermal decomposition of trichloromethanol CCl_3OH to phosgene $COCl_2$ and hydrogen chloride HCl:

$$CCl_3OH \rightarrow COCl_2 + HCl \quad (3)$$

was investigated experimentally and theoretically [20–24, 29]. Several smog-chamber experiments show the kinetic behavior of CCl_3OH to be very similar to that of CF_3OH. The measured rate of CCl_3OH decay strongly depends on the geometry and surface of the reactor walls, which implies a heterogeneous mechanism of CCl_3OH decomposition. A value of 1.05×10^{-2} s^{-1} was estimated [22] as the upper limit of the overall rate coefficient k_3 at room temperature. This is in serious disagreement with the results of theoretical investigations [21]. The height of the energy barrier for the thermal dissociation of CCl_3OH calculated at different levels of theory is high, over 125 kJ mol^{-1}, and corresponds to a value of the first-order rate coefficient for CCl_3OH decomposition which is 8 orders of magnitude lower than that estimated experimentally.

There is no experimental information on the kinetics of the unimolecular decomposition of CBr_3OH:

$$CBr_3OH \rightarrow COBr_2 + HBr. \quad (4)$$

However, the structural similarity of CBr_3OH to CCl_3OH and CF_3OH suggests that the mechanism of CBr_3OH decomposition is likely analogous to reactions (2) and (3).

Experimental investigations showed that the introduction of water vapor into the reaction chamber leads to acceleration of the decomposition of CF_3OH [10]. The incorporation of CF_3OH into water droplets or its decomposition on aerosols is thought to dominate the loss processes of atmospheric CF_3OH. The results of *ab initio* calculations show the existence of a lower energy pathway on the potential energy surface available in the reaction systems CF_3OH+H_2O, CCl_3OH+H_2O, and CBr_3OH+H_2O [14, 29]. An analysis of the calculated potential energy surface for the CY_3OH+H_2O (Y = F, Cl and Br) reaction systems allows an explanation of the role of water in the decomposition of CY_3OH molecules [29]. A water molecule approaching a CY_3OH molecule is oriented in such a manner that enables the formation of a six-atom ring structure which supports the transport and exchange of hydrogen atoms inside the ring.

It would seem that hydrogen halides may play a similar role in the catalytic decomposition of CY_3OH. Therefore we performed *ab initio* calculations of the potential energy surface of the CY_3OH+HX (where X, Y = F, Cl, and Br) reaction system

$$CY_3OH + HX \rightarrow CY_2O + HY + HX \quad (5)$$

to gain insight into the reaction mechanism. Results of the calculations will provide the molecular information necessary for computational methods used to evaluate the reaction rate coefficients.

Computational details

The perhalogenated alcohols CF_3OH, CCl_3OH, and CBr_3OH have been studied theoretically quite extensively using quantum mechanical *ab initio* methods at various levels of theory. Because the results obtained by the G2 method [33] reproduce the structural parameters and molecular properties [25–29] of CY_3OH molecules very well, we decided to use this level of theory in our investigations. All quantum mechanical *ab initio* calculations were carried out using the Gaussian 03 program [34] package. Electron correlation was estimated by Møller-Plesset perturbation theory at the second (MP2) and up to the fourth order including all single, double, triple, and quadruple excitations (MP4SDTQ). The frozen core approximation was kept throughout.

The rate coefficients of the reactions studied were analyzed in terms of conventional transition state theory (TST) [35, 36] according to the equation:

$$k_{TST} = \kappa_T \sigma \frac{k_B T}{h} \exp\left(\frac{\Delta S^{\neq}}{R}\right) \exp\left(-\frac{\Delta H^{\neq}}{RT}\right), \quad (6)$$

where κ_T is the tunneling correction factor, σ a symmetry factor related to degeneracy of the reaction path, and k_B and h the Boltzmann and Planck constants, respectively.

$\Delta S^{\neq}$ is the activation entropy and $\Delta H^{\neq}$ the activation enthalpy of the reaction under investigation. Vibrational and rotational contributions to the thermodynamic functions were derived by the classical harmonic-oscillator rigid-rotor approximation (no free or internal rotation was considered).

The rate coefficient calculation of a reaction with a high energy barrier should take into consideration a tunneling effect. This is usually inserted in the rate coefficient by the tunneling correction factor κ_T as:

$$k = \kappa_T \, k_{TST}. \tag{7}$$

Including the tunneling effect may distinctly improve the values of the calculated rate coefficients, especially at low temperatures. The calculated rate coefficients are given in Tables 4, 5, 6. The tunneling correction factors κ_T were evaluated from the simple Wigner's expression [35]

$$\kappa_T \cong 1 - \frac{1}{24}\left(\frac{h\nu^{\neq}}{k_B T}\right)^2, \tag{8}$$

with the imaginary frequencies $\nu^{\neq}$ of the transition state obtained in the geometry optimization performed at a higher level of theory, i.e., from MP2/6-31G(d) calculations.

Results and discussion

It is well known that the G2 method [33] well reproduces the structural parameters and molecular properties of a wide group of organic compounds. The halogenated alcohols have become the subject of theoretical investigations at several levels of theory because of their possible role in the destruction of atmospheric ozone. Results of calculations show a distinct advantage of the G2 approach, which better reproduces the molecular properties of this class of compounds. The reliable values of the thermochemical properties and vibrational frequencies obtained by G2 methodology for perhalogenated methanols by us [16–18, 24, 29] and other authors [26–28] favor the use of this level of theory for a description of the structural parameters of the investigated molecular systems.

The geometries of the molecular structures taking part in the reaction mechanism CY_3OH+HX, (X, Y = F, Cl and Br) were optimized independently at the SCF/6-31G(d) and MP2/6-31G(d) levels. The molecular arrangements and definitions of the structural parameters used in the geometry optimization are given in Fig. 1.

At each level of theory the potential energy surface was explored independently for the possible existence of transition states and intermediate complexes. The optimized geometrical parameters at the MP2/6-31G(d) level, the harmonic vibrational frequencies (scaled by 0.8929) obtained at the SCF/6-31G(d) level, and the total G2 energies for the CY_3OH, CY_2O, and $CY_3OH\ldots HX$ structures are given in Tables 1, 2 and 3. The structural parameters of the HX molecules were published elsewhere [17].

Homogenous decomposition of CF_3OH

The most stable structure of CF_3OH appears to possess a staggered conformation with C_s molecular symmetry. Trifluoromethanol is a molecular structure with an unusually strong CF_3O–H bond. The bond dissociation energy of CF_3O–H is distinctly greater than that of CH_3OH and comparable to or even slightly greater than that of HO-H in water. This anomalously large CF_3O-H bond strength is usually attributed to the negative hyperconjugation effect of the CF_3 group [37]. Except for the C-F bond lengths, the geometrical parameters of CF_3OH are very similar to those of methanol.

The saddle point $CF_3OH^{\neq}$, denoted by TS1F, for the decomposition $CF_3OH \rightarrow CF_2O+HF$ also has C_s symmetry, with the C-F_1 and O-H_0 bonds oriented almost in parallel and located in the symmetry plane F_1COH_0. The lengths of the breaking bonds (O-H_0: 1.25 Å, C-F_1: 1.72 Å) are 30% longer than the corresponding bonds in CF_3OH. The thermal decomposition of $CF_3OH \rightarrow CF_2O+HF$ is an almost thermoneutral process, related to the very high energy barrier of 157 kJ mol^{-1} obtained at the G2 level. This implies either small values of the rate coefficient or its strong dependence on temperature.

The pre-reaction adducts $CF_3OH...HX$, designated as MC1F-HX, are the most stable structures in all the studied CF_3OH+HX reaction systems. The thermal stabilities of the MC1F-HX complexes with respect to the corresponding reactants are very similar and cover a range of 45-50 kJ mol^{-1} at 0 K. The geometrical parameters of these hydrogen-bonding complexes retain the values which appear in the isolated reactants, i.e., the CF_3OH and HX molecules. Only the contact bonds F_1-H and XH_0 are considerably longer than the analogous H-X bonds in the hydrogen halides. The binding energy of the pre-adduct, CF_3OH-HX (MC1F-HX) is described by the strength of the formed F...H and H_o...X hydrogen bonds. The dissociation energy of MC1F-HX complexes toward reactants increases as $CF_3OH..BrH < CF_3OH...ClH < CF_3OH...FH$, which is in agreement with the strength of the H-X bonds, H-Br < H-Cl < H-F.

The transition states $(CF_3OH..HX)^{\neq}$, denoted by TS2F-HX, describe the decomposition of trifluoromethanol in the gas phase in the presence of the respective hydrogen halide molecule HX. Weakening of the H-X bond, which appears when an HX molecule approaches CF_3OH, enables the formation of a six-atom (C...F_1...H…X…

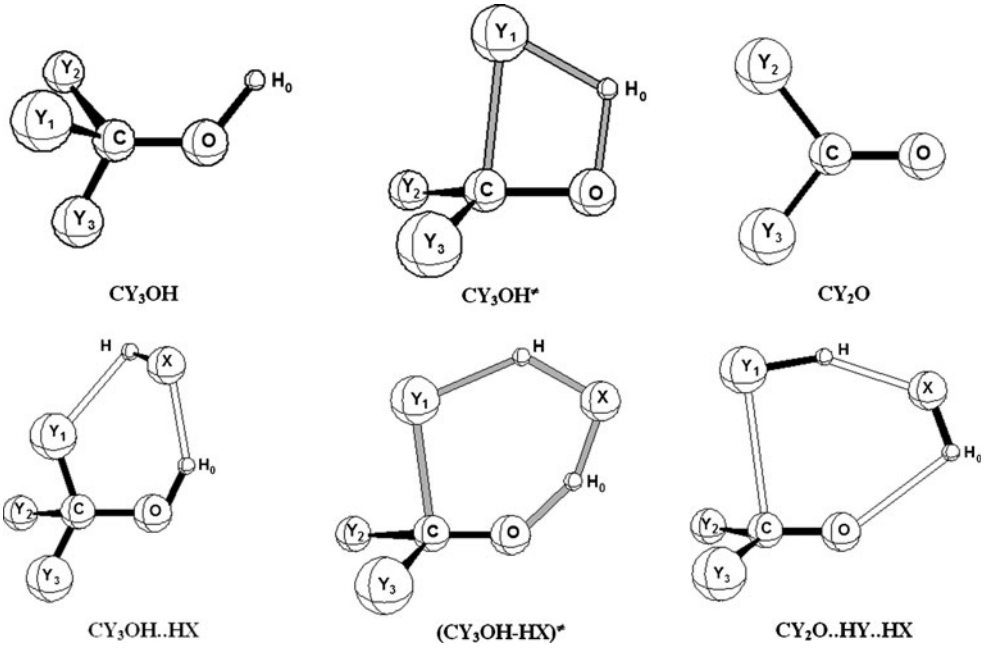

Fig. 1 Definition of the geometrical parameters of the molecular structures taking part in the mechanism of the CY_3OH+HX reactions

H_0…O) ring structure. This structure supports the abstraction of F_1 and H_0 atoms from the alcohol and plays an important role in the reaction mechanism of the HX-catalyzed decomposition of CF_3OH. A comparative analysis of the structural parameters shows that the transition states $(CF_3OH..HX)^{\neq}$ are considerably looser molecular structures than TS1F. The angular parameters of TS2F-HX, especially of F_1CO and COH_0, are very close to those of the isolated CF_3OH molecule. The length of the critical bond H…F_1, which is 2.44 Å in the CF_3OH molecule, undergoes only a slight change in the molecular structures of the transition states TS2F-HX to 2.29 Å, 2.46 Å, and 2.52 Å for TS2F-HF, TS2F-HCl, and TS2F-HBr, respectively. This is in contrast to TS1F, whose H_0…F bond length of 1.19 Å is half that of the TS2F-HX structures. That is why the formation of the TS2F-HX transition states requires considerably fewer changes in the structures of the reactants than the formation of TS1F. Consequently, the transformation of the reactant(s) into the respective transition state in the CF_3OH+HX reaction system proceeds easily and requires less energy than the thermal decomposition of CF_3OH.

The post-reaction adducts CF_2O...HF...HX, denoted by MC2F-HX, are molecular structures which consist of three subunits, CF_2O, HF, and HX, bonded in a molecular complex. The geometrical parameters of these subunits are very close to those of the isolated molecules. The contact distances C…F_1, O…H_0, and H_0…X calculated at the MP2/6-31G(d) level are almost twice those in the isolated reactants. Decay of the post-reaction adducts MC2F-HX yields the final reaction products, CF_2O and HF.

The reaction mechanism of the HX-accelerated decomposition of CF_3OH consists of three elementary steps:

$$CF_3OH + HX \leftrightarrows CF_3OH...HX \leftrightarrows CF_2O...HF...HX \rightarrow CF_2O + HF + HX. \quad (9)$$

The first and third elementary processes are recombination and unimolecular dissociation, while the second is related to an energy barrier.

The profiles of the potential energy surface calculated for the HX-accelerated decomposition of CF_3OH are shown in Fig. 2. The first elementary step of the reaction mechanism is related to the formation of the pre-reaction adduct MC1F-HX. The next step leads, via TS2F-HX, directly to the other molecular complex, MC2F-HX, which dissociates to the final reaction products. This mechanism explains the catalytic influence of the HX molecule, which acts as a molecular agent in promoting the transport and exchange of hydrogen atoms inside the formed ring. An analysis of the structural parameters shows that the formation of TS2F-HX transition states requires fewer changes in the structure of the reactants than the formation of TS1F. This results in a decrease in the activation barrier. The high energy barrier of 157 kJ mol^{-1} for the thermal dissociation of CF_3OH becomes distinctly smaller under the influence of hydrogen halides, achieving values of 66 kJ mol^{-1}, 94 kJ mol^{-1}, and 93 kJ mol^{-1} for the CF_3OH +HF, CF_3OH+HCl, and CF_3OH+HBr reactions, respectively. The presence of HF leads to the greatest reduction in the activation barrier, by over 90 kJ mol^{-1}, whereas HCl and HBr lower the height of the energy barrier by a little less than 65 kJ mol^{-1}.

Table 1 Molecular properties of the structures taking part in the reaction mechanism of the thermal decomposition of trifluoromethanol in the presence of hydrogen halides [a)]

	CF_3OH	TS1F	CF_2O	MC1F-HF	TS2F-HF	MC2F-HF		MC1F-HCl	TS2F-HCl	MC2F-HCl	MC1F-HBr	TS2F-HBr	MC2F-HBr
CO	1.3511	1.2628	1.1871	1.3362	1.2492	1.1964	CO	1.3436	1.2559	1.1930	1.3437	1.2567	1.1930
OH_0	0.9741	1.2545		0.9823	1.2345	1.8283	OH_0	0.9774	1.1084	2.0747	1.3517	1.8176	2.1137
CF_1	1.3520	1.7186	1.3277	1.3814	1.7286	1.3122	CF_1	1.3651	1.8115	1.3168	0.9784	1.0968	2.5439
CF_2	1.3520	1.3168	1.3277	1.3490	1.3139	1.3162	CF_2	1.3513	1.2967	1.3201	1.3635	1.2958	1.3168
CF_3	1.3317	1.3168		1.3293	1.3274	2.5098	CF_3	1.3305	1.3078	2.5498	1.3317	1.3057	1.3209
XH_0				1.8526	1.1428	0.9500	XH_0	2.5365	1.7328	1.2874	2.5840	1.8996	1.4434
XH				0.9430	1.1708	1.7026	XH	1.2821	1.7167	2.4136	1.4375	1.8697	2.4744
COH_0	108.1404	80.7211		107.5284	107.7525	116.6439	COH_0	108.3524	108.7918	124.4120	108.0407	109.1370	121.6622
F_1CO	112.1963	91.0308	126.2625	111.7254	105.3463	125.3047	F_1CO	112.2032	103.9446	125.6872	112.7477	104.1826	98.4587
F_2CO	112.1963	121.7898	126.2625	113.4601	119.5416	125.4141	F_2CO	112.7292	118.7751	125.6110	112.2218	118.5023	125.7501
F_3CO	108.3109	121.7898		109.7308	120.5603	94.5331	F_3CO	108.9136	121.3395	97.5638	108.8981	121.4593	125.5398
XH_0O				147.3703	153.7427	147.1261	XH_0O	149.8158	154.8745	148.2953	154.5783	153.4524	145.5588
HXH_0				93.4586	88.0866	96.1510	HXH_0	84.9027	70.6419	82.7578	83.8001	67.7053	80.1448
F_1COH_0	59.8927	0.0000		−54.1173	33.0892	136.3312	F_1COH_0	−60.5542	50.9202	132.8750	−60.3128	55.2916	45.3080
F_2COH_0	−59.8927	106.4701		64.6071	143.6113	−48.4347	F_2COH_0	58.7692	158.8719	−50.8417	59.1060	162.5715	139.5997
F_3COH_0	180.0000	−106.4701		−173.3824	−74.5284	38.4809	F_3COH_0	179.7865	−54.1423	38.6004	178.8617	−50.0116	−44.3252
XH_0OC				29.0462	−31.4623	−38.7326	XH_0OC	32.8060	−42.5369	−38.6876	−20.3991	−43.3396	−40.0679
HXH_0O				5.0758	6.2710	1.1473	XFH_0O	−2.1988	6.0645	3.6758	−12.2950	4.6111	0.4078
ν_1	235	1758 i [b)]	563	45	1397 i [b)]	7	ν_1	23	842 i [b)]	10	30	652 i [b)]	11
ν_2	428	260	610	95	115	74	ν_2	51	80	69	38	71	54
ν_3	441	336	779	151	179	89	ν_3	67	213	74	73	175	76
ν_4	583	537	977	221	232	123	ν_4	103	258	86	85	239	78
ν_5	607	551	1306	345	277	169	ν_5	204	326	97	220	327	103
ν_6	617	684	1952	407	327	204	ν_6	324	360	124	366	351	124
ν_7	889	823		435	367	341	ν_7	430	550	192	431	552	161
ν_8	1123	916		528	462	468	ν_8	451	566	255	469	564	242
ν_9	1235	981		591	503	519	ν_9	586	602	294	588	600	335
ν_{10}	1324	1389		610	718	569	ν_{10}	607	755	458	609	750	492
ν_{11}	1414	1617		617	1024	612	ν_{11}	617	857	568	617	828	568
ν_{12}	3653	1973		886	1073	736	ν_{12}	888	966	612	888	965	612
ν_{13}				1140	1243	785	ν_{13}	1131	1090	780	1139	1090	779
ν_{14}				1217	1288	996	ν_{14}	1222	1252	989	1225	1248	987
ν_{15}				1343	1337	1351	ν_{15}	1330	1503	1335	1332	1500	1332
ν_{16}				1439	1532	1905	ν_{16}	1419	1594	1922	1424	1586	1925
ν_{17}				3590	1790	3696	ν_{17}	2837	2017	2804	2498	1975	2485
ν_{18}				3836	3101	3758	ν_{18}	3630	2790	3816	3620	2761	3797
E_0(G2)	−413.03877	−412.97890	−312.69122	−513.40782	−513.36352	−513.40605	E_0(G2)	−873.39694	−873.34310	−873.39291	−2986.22914	−2986.17669	−2986.22442

[a)] G2 molecular parameters: geometrical structure optimized at the MP2/6-31G(d) level, (bond lengths in Å, valence and dihedral angles in degrees), the SCF/6-31G(d) vibrational frequencies ν_i (cm^{-1}) are scaled by 0.8929 and the total G2-energies are in a.u. at 0 K (ZPE included)

[b)] the unscaled MP2/6-31G(d) vibrational frequencies (cm^{-1})

Table 2 Molecular properties of the structures taking part in the reaction mechanism of the thermal decomposition of trichloromethanol in the presence of hydrogen halides [a)]

	CCl_3OH	TS1Cl	CCl_2O	MC1Cl-HF	TS2Cl-HF	MC2Cl-HF		MC1Cl-HCl	TS2Cl-HCl	MC2Cl-HCl	MC1Cl-HBr	TS2Cl-HBr	MC2Cl-HBr
CO	1.3684	1.2773	1.1949	1.3516	1.2576	1.2063	CO	1.3599	1.2697	1.2019	1.3595	1.2731	1.2023
OH_0	0.9781	1.1215		0.9864	1.1480	1.8316	OH_0	0.9813	1.0767	2.0622	0.9825	1.0704	2.1004
CCl_1	1.7916	2.4629	1.7447	1.8209	2.4895	3.8608	CCl_1	1.8041	2.4677	3.6654	1.7932	2.4135	3.6788
CCl_2	1.7916	1.7062	1.7447	1.7924	1.7008	1.7254	CCl_2	1.7923	1.6952	1.7312	1.8039	1.6999	1.7310
CCl_3	1.7586	1.7002		1.7574	1.7221	1.7273	CCl_3	1.7591	1.7108	1.7346	1.7594	1.7144	1.7354
XH_0				1.8033	1.2320	0.9471	XH_0	2.4539	1.7941	1.2873	2.5402	1.9496	1.4433
XH				0.9426	1.0869	1.8868	XH	1.2822	1.5764	2.6444	1.4377	1.7370	2.6582
COH_0	108.1514	97.4696		108.4031	110.8941	120.3710	COH_0	108.7689	112.1580	127.8633	108.5364	111.9019	120.2369
Cl_1CO	111.0518	82.3137	123.8843	111.0200	97.2495	125.3047	Cl_1CO	111.2129	98.6362	81.3511	111.5708	100.2562	84.0893
Cl_2CO	111.0518	120.5714	123.8843	111.9807	117.9519	122.7581	Cl_2CO	111.5624	116.4558	123.2629	111.2190	115.8432	123.3256
Cl_3CO	106.4187	119.6577		107.6396	120.4954	123.4709	Cl_3CO	106.8780	120.5878	123.5679	106.9229	120.1743	123.4823
XH_0O				159.5461	158.1406	157.8249	XH_0O	167.1854	157.0780	160.7682	168.3684	155.8212	155.4455
HXH_0				100.5677	93.7383	98.7658	HXH_0	93.8852	75.3718	82.7341	88.3763	72.0231	80.7067
Cl_1COH_0	60.1553	5.1592		−59.8179	50.3953	136.3312	Cl_1COH_0	−60.8981	58.6260	59.5224	−58.7771	62.5065	63.2891
Cl_2COH_0	−60.1553	94.5080		59.7955	157.7705	167.0485	Cl_2COH_0	59.3151	164.8041	158.3373	61.4036	169.0922	−18.2226
Cl_3COH_0	180.0000	−110.9961		−178.9518	−50.7549	−13.5368	Cl_3COH_0	179.6744	−44.5096	−22.3496	−179.1352	−42.6695	162.4286
XH_0OC				30.4944	−51.6826	−49.0143	XH_0OC	50.7926	−60.8933	−65.9690	−11.0272	−55.4111	−43.8676
HXH_0O				5.3143	7.0703	−19.7379	$XClH_0O$	−18.1145	13.5982	2.1824	−19.9102	7.0723	−21.7508
ν_1	234	1611 i [b)]	295	45	1397 i [b)]	7	ν_1	23	842 i [b)]	10	30	652 i [b)]	11
ν_2	245	72	445	95	115	74	ν_2	51	80	69	38	71	54
ν_3	324	219	565	151	179	89	ν_3	67	213	74	73	175	76
ν_4	342	282	581	221	232	123	ν_4	103	258	86	85	239	78
ν_5	393	320	878	345	277	169	ν_5	204	326	97	220	327	103
ν_6	414	424	1856	407	327	204	ν_6	324	360	124	366	351	124
ν_7	526	539		435	367	341	ν_7	430	550	192	431	552	161
ν_8	798	593		528	462	468	ν_8	451	566	255	469	564	242
ν_9	802	961		591	503	519	ν_9	586	602	294	588	600	335
ν_{10}	1143	1185		610	718	569	ν_{10}	607	755	458	609	750	492
ν_{11}	1297	1399		617	1024	612	ν_{11}	617	857	568	617	828	568
ν_{12}	3619	2612		886	1073	736	ν_{12}	888	966	612	888	965	612
ν_{13}				1140	1243	785	ν_{13}	1131	1090	780	1139	1090	779
ν_{14}				1217	1288	996	ν_{14}	1222	1252	989	1225	1248	987
ν_{15}				1343	1337	1351	ν_{15}	1330	1503	1335	1332	1500	1332
ν_{16}				1439	1532	1905	ν_{16}	1419	1594	1922	1424	1586	1925
ν_{17}				3590	1790	3696	ν_{17}	2837	2017	2804	2498	1975	2485
ν_{18}				3836	3101	3758	ν_{18}	3630	2790	3816	3620	2761	3797
E_0(G2)	−1492.98743	−1492.93343	−1032.66305	−513.40782	−513.36352	−513.40605	E_0(G2)	−873.39694	−873.34310	−873.39291	−2986.22914	−2986.17669	−2986.22442

[a)] G2 molecular parameters: geometrical structure optimized at the MP2/6-31G(d) level, (bond lengths in Å, valence and dihedral angles in degrees), the SCF/6-31G(d) vibrational frequencies ν_i (cm^{-1}) are scaled by 0.8929 and the total G2-energies are in a.u. at 0 K (ZPE included)

[b)] the unscaled MP2/6-31G(d) vibrational frequencies (cm^{-1})

Table 3 Molecular properties of the structures taking part in the reaction mechanism of the thermal decomposition of tribromomethanol in the presence of hydrogen halides [a)]

	CBr_3OH	TS1Br	CBr_2O	MC1Br-HF	TS2Br-HF	MC2Br-HF		MC1Br-HCl	TS2Br-HCl	MC2Br-HCl	MC1Br-HBr	TS2Br-HBr	MC2Br-HBr
CO	1.3624	1.2710	1.1900	1.3429	1.2506	1.2019	CO	1.3523	1.2618	1.1975	1.3513	1.2643	1.1976
OH_0	0.9801	1.1504		0.9907	1.2010	1.8881	OH_0	0.9843	1.1184	2.1250	0.986	1.1076	2.1768
CBr_1	1.9775	2.5714	1.9309	2.0194	2.5810	3.3625	CBr_1	2.0028	2.5899	3.3773	1.9758	2.5660	3.3976
CBr_2	1.9775	1.8919	1.9309	1.9762	1.8877	1.9041	CBr_2	1.9739	1.8785	1.9136	2.0028	1.8805	1.9199
CBr_3	1.9364	1.8831		1.9344	1.9179	1.9123	CBr_3	1.9361	1.9000	1.9197	1.9372	1.9000	1.9145
XH_0				1.7775	1.1735	0.9454	XH_0	2.4564	1.7020	1.2860	2.5067	1.8625	1.4415
XH				0.9467	1.1100	1.9679	XH	1.2858	1.6104	2.7530	1.4411	1.7748	2.6901
COH_0	107.9101	98.3400		108.153	110.2951	113.3531	COH_0	109.1116	111.8855	116.0897	108.9416	111.5832	115.4825
Br_1CO	111.4618	83.4133	124.1137	111.4428	99.3654	91.1972	Br_1CO	111.8952	100.2924	95.9871	112.4793	101.1643	97.0362
Br_2CO	111.4618	120.7480	124.1137	112.6872	118.5678	123.4623	Br_2CO	112.2543	117.1200	123.8153	111.8995	116.6469	123.6585
Br_3CO	107.0317	120.0365		108.4920	120.0673	123.2083	Br_3CO	107.5833	120.5385	123.5064	107.5656	120.4932	123.7423
XH_0O				156.5017	159.4436	149.6627	XH_0O	158.7438	159.8903	157.6404	161.2245	158.8981	148.7305
HXH_0				98.2152	95.5661	158.4755	HXH_0	80.5258	77.5543	85.4690	79.1114	74.5401	82.8781
Br_1COH_0	60.0759	5.1414		−61.5266	50.4033	58.3930	Br_1COH_0	−66.0483	58.6913	60.6353	−55.4448	62.7997	61.9441
Br_2COH_0	−60.0759	−95.0590		57.4842	158.8295	153.0263	Br_2COH_0	53.9532	165.5191	152.2627	64.6418	169.5117	−26.1592
Br_3COH_0	180.0000	110.7385		179.5520	−52.1406	−27.0436	Br_3COH_0	175.0639	−44.9415	−28.0199	−176.4778	−41.9118	154.1595
XH_0OC				27.1319	−50.9266	−44.6755	XH_0OC	43.3351	−58.9397	−53.3750	−13.0235	−51.0571	−24.5967
HXH_0O				10.5863	6.6792	−16.1968	$XBrH_0O$	−5.6268	11.4645	−2.4679	−27.0558	1.5180	−31.9056
ν_1	148	1770 i [b)]	179	31	1350 i [b)]	6	ν_1	17	1186 i [b)]	13	28	935 i [b)]	24
ν_2	151	45	347	90	30	18	ν_2	41	53	25	39	50	27
ν_3	211	132	410	127	67	42	ν_3	63	61	30	55	70	37
ν_4	264	192	515	150	88	53	ν_4	142	86	40	133	87	43
ν_5	308	240	751	158	148	91	ν_5	150	120	49	151	114	50
ν_6	368	340	1861	209	188	121	ν_6	157	184	70	154	170	58
ν_7	398	430		239	278	181	ν_7	210	192	114	209	191	179
ν_8	693	529		301	353	257	ν_8	219	265	177	219	218	185
ν_9	697	825		332	431	314	ν_9	291	372	179	295	366	195
ν_{10}	1127	1165		395	461	354	ν_{10}	314	436	207	322	436	275
ν_{11}	1285	1378		416	796	396	ν_{11}	396	453	284	397	478	325
ν_{12}	3608	2512		578	838	425	ν_{12}	415	718	356	468	652	354
ν_{13}				673	945	504	ν_{13}	682	802	419	682	780	417
ν_{14}				711	967	539	ν_{14}	702	841	518	704	835	518
ν_{15}				1152	1321	785	ν_{15}	1135	938	770	1137	926	767
ν_{16}				1339	1466	1812	ν_{16}	1291	1291	1831	1309	1294	1835
ν_{17}				3523	1644	2469	ν_{17}	2826	1509	2493	2497	1487	2479
ν_{18}				3802	2229	3778	ν_{18}	3582	2753	2814	3568	2822	2492
E_0(G2)	−7831.48792	−7831.43747	−5258.33155	−7931.84527	−7931.81532	−7931.86348	E_0(G2)	−8291.83436	−8291.80145	−8291.85273	−10404.66560	−10404.63507	−10404.68319

[a)] G2 molecular parameters: geometrical structure optimized at the MP2/6-31G(d) level, (bond lengths in Å, valence and dihedral angles in degrees), the SCF/6-31G(d) vibrational frequencies ν_i (cm^{-1}) are scaled by 0.8929 and the total G2-energies are in a.u. at 0 K (ZPE included)

[b)] the unscaled MP2/6-31G(d) vibrational frequencies (cm^{-1})

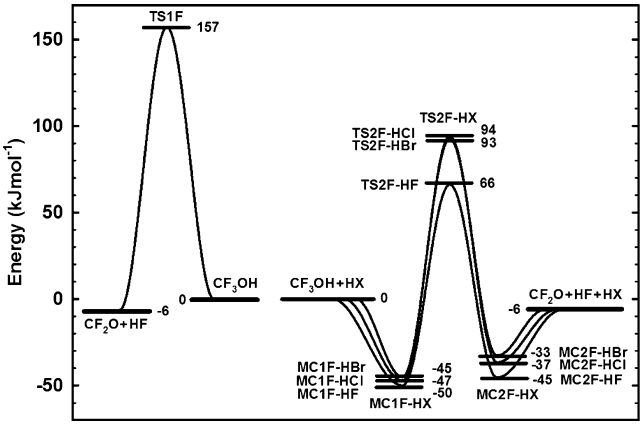

Fig. 2 Schematic energy profile for the decomposition of CF_3OH in the absence (left side) and presence (right side) of hydrogen halides, HX. The energies are calculated at the G2 level including zero-point energy corrections

Homogenous decomposition of CCl_3OH

The optimized structural parameters, vibrational frequencies, and G2-total energies of the molecular structures taking part in the thermal decomposition of CCl_3OH are given in Table 2. The calculations show that the most stable structure of CCl_3OH appears to possess a staggered conformation with C_s molecular symmetry, like CF_3OH. The only significant difference in the geometrical parameters of CF_3OH and CCl_3OH is related to the C-F and C-Cl bond lengths. The other structural parameters, bond lengths, and angular parameters of CF_3OH and CCl_3OH are very close to those of the methanol molecule.

The transition state $CCl_3OH^{\neq}$, denoted by TS1Cl, describes the unimolecular dissociation of CCl_3OH according to the reaction $CCl_3OH \rightarrow CCl_2O+HCl$. Some structural parameters of TS1Cl differ distinctly from their counterparts in the TS1F structure. TS1Cl has a symmetry of C_1 point group. The C-Cl_1 contact distance of 2.46 Å is 0.74 Å longer than the C-F_1 bond in the $CF_3OH^{\neq}$ structure, whereas the O-H_0 bond length is a little shorter than that in $CF_3OH^{\neq}$. The valence angles Cl-C-O and C-O-H_0 differ distinctly from the F-C-O and C-O-H_0 angles in the TS1F structure. The relative total energy of $CCl_3OH^{\neq}$ with respect to CCl_3OH calculated at the G2 level is found to be 142 kJ mol^{-1}. This value corresponds to the height of the energy barrier for the unimolecular decomposition of CCl_3OH at 0 K.

The pre-reaction adducts CCl_3OH...HX, designated as MC1Cl-HX, are hydrogen-bonding complexes with a thermal stability toward the corresponding reactants of 15-20 kJ mol^{-1} at 0 K. This is less than half that of the heat of formation of the corresponding MC1F-HX from the reactants CF_3OH+HX. The most stable structure is CCl_3OH...HF (MC1Cl-HF) and the least is CCl_3OH…HBr (MC1Cl-HBr). The geometrical parameters of the MC1Cl-HX adducts are very close to those in the isolated reactants, i.e., of the CCl_3OH, HF, HCl, and HBr molecules.

The transition states $(CCl_3OH..HX)^{\neq}$, denoted by TS2Cl-HX, describe the decomposition of trichloromethanol accelerated by the hydrogen halides HF, HCl, and HBr. The relative G2 energies of TS2Cl-HX toward the respective reactants were calculated as 65, 74, and 65 kJ mol^{-1} at 0 K for TS2Cl-HF, TS2Cl-Cl, and TS2Cl-Br, respectively. The geometrical configuration of the $(CCl_3OH..HX)^{\neq}$ structures are similar to their counterparts $(CF_3OH..HX)^{\neq}$, but the lengths of the corresponding bonds differ significantly. Only the lengths of the O-H_0 bond in TS2Cl-HX are slightly shorter than those in the transition states TS2F-HX. The other bond lengths of the TS2Cl-HX structures are larger compared with TS2F-HX. A shift of HX molecules in the direction of the abstracted chlorine atom Cl_1 changes the orientation of the CCl_3OH skeleton of TS2Cl-HX only slightly compared with the pre-reaction adducts MC1Cl-HX.

The post-reaction adducts CCl_2O…HCl…HX, denoted by MC2Cl-HX, are the most stable molecular structures in the CCl_3OH+HF/HCl/HBr reaction systems. The molecular complexes MC2Cl-HX are loose molecular structures with long contact distances between the subunits CCl_2O, HCl, and HX. The dissociation energy of the MC2Cl-HX complexes to the final reaction products calculated at the G2 level are found to be 34, 28, and 24 kJ mol^{-1} at 0 K for MC2Cl-HF, MC2Cl-HCl, and MC2Cl-HBr, respectively.

The profiles of the potential energy surface for the decomposition of CCl_3OH (+HF/HCl/HBr) calculated at the G2 level are shown in Fig. 3. The thermal decomposition of CCl_3OH is an exothermic reaction at all the

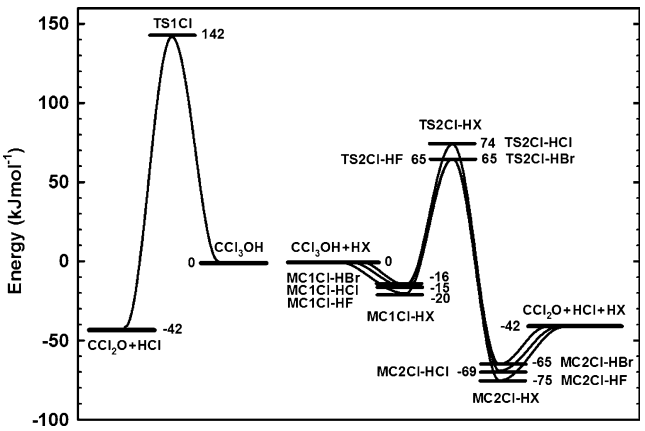

Fig. 3 Schematic energy profile for the decomposition of CCl_3OH in the absence (left side) and presence (right side) of hydrogen halides, HX. The energies are calculated at the G2 level including zero-point energy corrections

temperatures considered in this study. The energy barrier for the thermal decomposition of CCl_3OH (reaction 3) calculated at the G2 level is high, 142 kJ mol^{-1}, at 0 K. This is 15 kJ mol^{-1} less than the analogous reaction of CF_3OH. A more complex reaction mechanism is postulated when the decomposition of CCl_3OH proceeds in the presence of hydrogen halides.

$$CCl_3OH + HX \leftrightarrows CCl_3OH...HX \leftrightarrows CCl_2O...HCl...HX \rightarrow CCl_2O + HCl + HX \quad (10)$$

The approach of the HX molecules to CCl_3OH leads to the formation of the CCl_3OH...HX (MC1Cl-HX) molecular complexes. However, the binding energies of the formed complexes between the hydrogen halides and trichloromethanol MC1Cl-HX are distinctly lower than those in the corresponding MC1F-HX intermediates. The reaction path then leads through the transition state TS2Cl-HX to another molecular complex, MC2Cl-HX, which finally dissociates into reaction products. The threshold energies for these pathways toward the reactants are distinctly lower than that for the unimolecular dissociation of CCl_3OH. Values of the reduction of the reaction barrier for the decay of CCl_3OH caused by the presence of HF, HCl, and HBr are found of 77, 68, and 77 kJ mol^{-1}, respectively.

Homogenous decomposition of CBr_3OH

The calculated properties of the molecular structures taking part in the reaction mechanism of the decomposition of CBr_3OH in the presence of HF, HCl, and HBr are gathered in Table 3. A staggered conformation with a symmetry of the C_s point group was found as the most stable molecular structure of CBr_3OH, like CF_3OH and CCl_3OH. Except for the C-Br bond lengths, the geometrical parameters of CBr_3OH are close to their counterparts in the CCl_3OH and CF_3OH molecules.

The saddle point $CBr_3OH^{\neq}$, denoted by TS1Br, for the unimolecular decomposition of CBr_3OH has C_1 symmetry, like the TS1Cl structure. All the bond lengths in $CBr_3OH^{\neq}$ are systematically longer than in $CF_3OH^{\neq}$ and $CCl_3OH^{\neq}$, whereas the angular parameters are very close to those in $CCl_3OH^{\neq}$. The energy barrier for the unimolecular dissociation $CBr_3OH \rightarrow CBr_2O+HBr$ calculated at the G2 level is 133 kJ mol^{-1} at 0 K.

The pre-reaction adducts CBr_3OH...HX, denoted by MC1Br-HX, are molecular complexes with a symmetry of C_s point group. The geometrical parameters of the subunits of MC1Br-HX, i.e., CBr_3OH and HX, are close to those in the isolated tribromomethanol and hydrogen halides. The formation of MC1Br-HX complexes is a less exothermic process than the formation of the corresponding MC1Cl-HX. The most stable is CBr_3OH...HF (MC1Br-HF). However, its dissociation energy toward the reactants CBr_3OH and HF is found to be 19 kJ mol^{-1} at 0 K. The formation of MC1Br-HF is thus a distinctly less exothermic process than the formation of MC1Cl-HF and MC1F-HF.

The transition states $(CBr_3OH..HX)^{\neq}$, designated as TS2Br-HX, are critical structures in the kinetic description of the decomposition of tribromomethanol in the presence of hydrogen halides, HX. The structural parameters of the transition states TS2Br-HX show similarity to the corresponding TS2Cl-HX structures. The angular parameters of TS2Br-HX and TS2Cl-HX are very close. However, except for the H_0-X and C-O bond lengths, the bonds of TS2Br-HX are considerably longer than their counterparts in TS2Cl-HX. The calculated energy barriers are 59, 70, and 68 kJ mol^{-1} at 0 K for the CBr_3OH+HF, CBr_3OH+HCl, and CBr_3OH+HBr reactions, respectively.

The post-reaction adducts CBr_2O…HBr…HX, designated MC2Br-HX, are loose structures with long contact distances between CBr_2O, HBr, and HX. The molecular complexes MC2Br-HX are the most stable structures in the CBr_3OH+HF/HCl/HBr reaction systems. The dissociation energy of the post-reaction complexes to the respective final reaction products cover a range of 14 - 23 kJ mol^{-1} at 0 K.

The mechanism of the decomposition of CBr_3OH was analyzed in terms of the profiles of the potential energy surface, which are shown in Fig. 4. The unimolecular decomposition of CBr_3OH is the most exothermic among the reactions under investigation. The energy barrier for the reaction $CBr_3OH \rightarrow CBr_2O+HBr$ is high, i.e., 132 kJ mol^{-1}, but lower than those derived for the unimolecular decomposition of CF_3OH and CCl_3OH. In the presence of the hydrogen halides HF, HCl, and HBr, the mechanism of

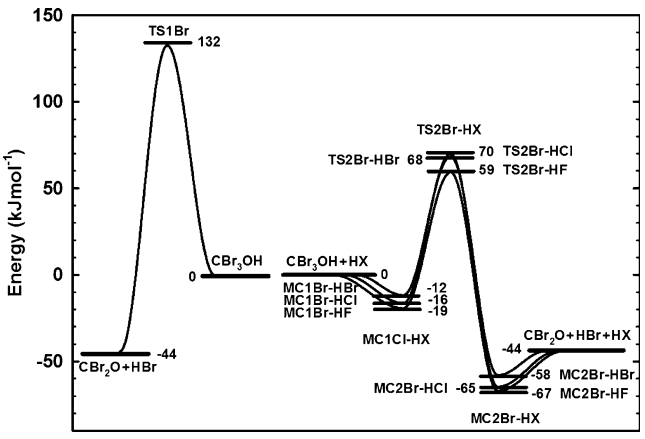

Fig. 4 Schematic energy profile for the decomposition of CBr_3OH in the absence (left side) and presence (right side) of hydrogen halides, HX. The energies are calculated at the G2 level including zero-point energy corrections

decomposition of CBr_3OH is complex and consists of three elementary steps.

$$CBr_3OH + HX \leftrightarrows CBr_3OH...HX \leftrightarrows CBr_2O...HBr...HX \rightarrow CBr_2O + HBr + HX \quad (11)$$

Intermediate complexes are formed during the reaction. The thermal stability of the molecular complexes with respect to the reactants (MC1Y-HX) and products (MC2Y-HX) decreases when Y changes in the series from F to Br. The reaction CBr_3OH+HF is related to the lowest energy barrier, i.e., 59 kJ mol^{-1} at 0 K, and is expected to be the fastest process among the reactions analyzed.

Rate coefficient calculations

The rate coefficients for the thermal decomposition of perhalogenated methanols were analyzed in terms of transition state theory. Let us use a superscript of the rate coefficient to denote the order of the reaction. In this way, $k^{(1)}$ is the rate coefficient for the first-order decomposition of CY_3OH and $k^{(2)}$ is related to the second-order reaction CY_3OH+HX (the subscript HX with the rate coefficient symbol $k_{HX}^{(2)}$ is used to distinguish the hydrogen halide reactant). The height of the energy barrier is clearly the major factor determining the magnitude of the rate coefficient and its dependence on temperature. The energy barriers, calculated at the G2 level, for the reactions $CY_3OH \rightarrow COY_2$+HY (where Y = F, Cl, and Br) are high, over 130 kJ mol^{-1}.

The calculated rate coefficient $k^{(1)}$ for the first-order decomposition of CF_3OH is very small, with 3.3×10^{-14} s^{-1} at room temperature. This corresponds to an atmospheric lifetime τ of CF_3OH with respect to its thermal decomposition of 10^6 years, which is a few orders of magnitude greater than the experimental estimates [1]. The rate coefficients for the unimolecular decomposition of CCl_3OH and CBr_3OH are considerably greater than for the decay of CF_3OH. The calculated $k^{(1)}$ at room temperature are 3.8×10^{-11} and 1.9×10^{-9} s^{-1} for the unimolecular dissociation of CCl_3OH and CBr_3OH, respectively. The rate coefficients $k^{(1)}$ can be considered as the high-pressure limiting rate coefficients $k_{diss\infty,}$ in the theory of unimolecular reactions. In the temperature range of 200-3000 K, the rate coefficient $k_{diss,\infty}$ for the unimolecular dissociation of the perhalogenated alcohols can be expressed in terms of three-parameter fits of the form $A\times(T/300)^n\times\exp(-E/T)$, as:

$$k_{diss,\infty}(CF_3OH) = 2.3 \times 10^{13} \times (T/300)^{0.52} \times \exp(-18550/T) \quad s^{-1} \quad (12)$$

$$k_{diss,\infty}(CCl_3OH) = 9.5 \times 10^{13} \times (T/300)^{0.27} \times \exp(-16860/T) \quad s^{-1} \quad (13)$$

$$k_{diss,\infty}(CBr_3OH) = 9.2 \times 10^{13} \times (T/300)^{0.20} \times \exp(-15680/T) \quad s^{-1} \quad (14)$$

The above equations reproduce the values of the theoretical rate coefficients given in Table 4, 5 and 6 with precision sufficient for kinetic modeling; the relative errors do not exceed 10%.

The atmospheric lifetimes of CCl_3OH and CBr_3OH corresponding to the calculated values of $k^{(1)}$ are many orders of magnitude greater than the upper limits measured experimentally. This strongly suggests that the decomposition of CF_3OH, CCl_3OH, and CBr_3OH in the atmosphere must proceed according to a different and considerably more efficient reaction mechanism.

In the presence of hydrogen halides, the mechanism of the decomposition of CF_3OH, CCl_3OH, and CBr_3OH is more complex due to the formation of the intermediate complexes MC1Y-HX and MC2Y-HX. If the total pressure is sufficiently high to enable efficient collision stabilization of the adducts, the kinetics of the decomposition of CY_3OH molecules should be considered in detail by advanced kinetic models [38–42]. The general equation, which takes into account rotational energy, can be derived from RRKM theory. According to this formalism, the rate coefficient $k_{exact}^{(2)}$ for the multistep decomposition of CY_3OH+HX can be expressed as:

$$k_{exact}^{(2)} = \frac{z}{hQ_{R-OH}Q_{HX}} \int_{V_{TS2Y-HX}}^{\infty} \sum_J W_{MC1Y-HX}(E,J) \times \frac{W_{TS2Y-HX}(E,J)}{W_{MC1Y-HX}(E,J)+W_{TS2Y-HX}(E,J)} \times \frac{W_{MC2Y-HX}(E,J)}{W_{MC2Y-HX}(E,J)+W_{TS2Y-HX}(E,J)} \times \exp(-E/RT)dE \quad (15)$$

where $Q_{R\text{-}OH}$ and Q_{HX} are the partition functions of the alcohol CY_3OH and hydrogen halide HX, respectively, with the center of mass partition function factored out of the product $Q_{R\text{-}OH}Q_{HX}$ and included in z together with the partition functions of those inactive degrees of freedom which are not considered by the sums of the states under the integral. $V_{TS2Y\text{-}HX}$ is the threshold energy toward the reactants CY_3OH+HX and $W_{TS2Y\text{-}HX}(E,J)$, $W_{MC1Y\text{-}HX}(E,J)$, and $W_{MC2Y\text{-}HX}(E,J)$ denote the sum of the states at energy less than or equal to E and with angular momentum J for the transition state TS2Y-HX and the activated complexes

Table 4 The rate coefficients calculated for the unimolecular ($k^{(1)}$) and the bimolecular HX-accelerated, $k_{HX}^{(2)}$ decomposition of CF_3OH

T (K)	κ_0 [a]	$k^{(1)}$ (s^{-1})	κ_{HF} [b]	$k_{HF}^{(2)}$ ($cm^3molecule^{-1}s^{-1}$)	κ_{HCl} [b]	$k_{HCl}^{(2)}$ ($cm^3molecule^{-1}s^{-1}$)	κ_{HBr} [b]	$k_{HBr}^{(2)}$ ($cm^3molecule^{-1}s^{-1}$)
200	7.67	9.08×10^{-28}	5.21	1.02×10^{-29}	2.53	1.15×10^{-37}	1.92	1.57×10^{-37}
250	5.27	1.24×10^{-19}	3.69	2.27×10^{-26}	1.98	7.35×10^{-33}	1.59	9.16×10^{-33}
300	3.96	3.28×10^{-14}	2.87	3.97×10^{-24}	1.68	1.22×10^{-29}	1.41	1.44×10^{-29}
350	3.18	2.43×10^{-10}	2.37	1.64×10^{-22}	1.50	2.51×10^{-27}	1.30	2.86×10^{-27}
400	2.67	1.95×10^{-7}	2.05	2.73×10^{-21}	1.38	1.40×10^{-25}	1.23	1.57×10^{-25}
450	2.32	3.54×10^{-5}	1.83	2.50×10^{-20}	1.30	3.29×10^{-24}	1.18	3.61×10^{-24}
500	2.07	2.29×10^{-3}	1.67	1.50×10^{-19}	1.25	4.19×10^{-23}	1.15	4.54×10^{-23}
600	1.74	1.20×10^{0}	1.47	2.33×10^{-18}	1.17	2.01×10^{-21}	1.10	2.13×10^{-21}
700	1.54	1.07×10^{2}	1.34	1.75×10^{-17}	1.13	3.36×10^{-20}	1.08	3.50×10^{-20}
800	1.42	3.12×10^{3}	1.26	8.32×10^{-17}	1.10	2.90×10^{-19}	1.06	2.98×10^{-19}
900	1.33	4.36×10^{4}	1.21	2.91×10^{-16}	1.08	1.60×10^{-18}	1.05	1.63×10^{-18}
1000	1.27	3.63×10^{5}	1.17	8.17×10^{-16}	1.06	6.49×10^{-18}	1.04	6.54×10^{-18}
1500	1.12	2.22×10^{8}	1.08	2.38×10^{-14}	1.03	5.48×10^{-16}	1.02	5.33×10^{-16}
2000	1.07	5.78×10^{9}	1.04	1.65×10^{-13}	1.02	6.36×10^{-15}	1.01	6.03×10^{-15}
3000	1.03	1.57×10^{11}	1.02	1.62×10^{-12}	1.01	1.01×10^{-13}	1.00	9.33×10^{-14}

[a] Wigner tunneling correction factor κ_0 calculated for the imaginary frequency of the transition state TS1F ($CF_3OH^{\neq}$)

[b] Wigner tunneling correction factor κ_{HX} calculated for the imaginary frequency of the respective transition state TS2F-HX $(CF_3OH..HX)^{\neq}$

for the unimolecular dissociations of MC1Y-HX and MC2Y-HX, respectively. All computational effort is then related to calculating the sum of the states, *W(E,J)*. This calculation depends on the level at which the conservation of angular momentum is considered and is discussed in detail in Refs. [40, 41].

However, if the adducts are not stabilized and can rapidly undergo subsequent processes, the TST rate coefficient k_{TST} is a very good approximation of the exact rate coefficient, especially at ambient temperatures [29]. Analysis of the results of the direct calculations of Brudnik et al. [29] shows that the difference between the rate

Table 5 The rate coefficients calculated for the unimolecular, $k^{(1)}$ and the bimolecular HX-accelerated, $k_{HX}^{(2)}$ decomposition of CCl_3OH

T (K)	κ_0 [a]	$k^{(1)}$ (s^{-1})	κ_{HF} [b]	$k_{HF}^{(2)}$ ($cm^3molecule^{-1}s^{-1}$)	κ_{HCl} [b]	$k_{HCl}^{(2)}$ ($cm^3molecule^{-1}s^{-1}$)	κ_{HBr} [b]	$k_{HBr}^{(2)}$ ($cm^3molecule^{-1}s^{-1}$)
200	6.59	1.97×10^{-23}	3.95	3.56×10^{-29}	3.87	8.67×10^{-32}	2.95	8.44×10^{-30}
250	4.58	4.63×10^{-16}	2.89	6.52×10^{-26}	2.84	5.65×10^{-28}	2.25	1.87×10^{-26}
300	3.49	3.77×10^{-11}	2.31	9.76×10^{-24}	2.28	2.05×10^{-25}	1.87	3.34×10^{-24}
350	2.83	1.21×10^{-7}	1.96	3.52×10^{-22}	1.94	1.43×10^{-23}	1.64	1.41×10^{-22}
400	2.40	5.13×10^{-5}	1.74	5.25×10^{-21}	1.72	3.56×10^{-22}	1.49	2.43×10^{-21}
450	2.11	5.69×10^{-3}	1.58	4.35×10^{-20}	1.57	4.47×10^{-21}	1.39	2.29×10^{-20}
500	1.90	2.46×10^{-1}	1.47	2.39×10^{-19}	1.46	3.48×10^{-20}	1.31	1.42×10^{-19}
600	1.62	7.05×10^{1}	1.33	3.21×10^{-18}	1.32	8.03×10^{-19}	1.22	2.33×10^{-18}
700	1.46	4.03×10^{3}	1.24	2.14×10^{-17}	1.23	8.08×10^{-18}	1.16	1.84×10^{-17}
800	1.35	8.45×10^{4}	1.19	9.26×10^{-17}	1.18	4.81×10^{-17}	1.12	9.08×10^{-17}
900	1.28	9.05×10^{5}	1.15	2.99×10^{-16}	1.14	2.01×10^{-16}	1.10	3.28×10^{-16}
1000	1.22	6.06×10^{6}	1.12	7.87×10^{-16}	1.12	6.53×10^{-16}	1.08	9.47×10^{-16}
1500	1.10	1.89×10^{9}	1.05	1.85×10^{-14}	1.05	2.94×10^{-14}	1.04	2.97×10^{-14}
2000	1.06	3.44×10^{10}	1.03	1.15×10^{-13}	1.03	2.55×10^{-13}	1.02	2.12×10^{-13}
3000	1.03	6.43×10^{11}	1.01	1.01×10^{-12}	1.01	3.08×10^{-12}	1.01	2.10×10^{-12}

[a] Wigner tunneling correction factor κ_0 calculated for the imaginary frequency of the transition state TS1Cl ($CCl_3OH^{\neq}$)

[b] Wigner tunneling correction factor κ_{HX} calculated for the imaginary frequency of the respective transition state TS2Cl-HX $(CCl_3OH..HX)^{\neq}$

Table 6 The rate coefficients calculated for the unimolecular, $k^{(1)}$ and the bimolecular HX-accelerated, $k^{(2)}_{HX}$ decomposition of CBr_3OH

T (K)	κ_0 [a]	$k^{(1)}$ (s^{-1})	κ_{HF} [b]	$k^{(2)}_{HF}$ ($cm^3molecule^{-1}s^{-1}$)	κ_{HCl} [b]	$k^{(2)}_{HCl}$ ($cm^3molecule^{-1}s^{-1}$)	κ_{HBr} [b]	$k^{(2)}_{HBr}$ ($cm^3molecule^{-1}s^{-1}$)
200	7.75	7.18×10^{-21}	4.93	1.79×10^{-27}	4.03	7.64×10^{-31}	2.89	6.26×10^{-31}
250	5.32	5.25×10^{-14}	3.52	1.67×10^{-24}	2.94	2.97×10^{-27}	2.21	2.17×10^{-27}
300	4.00	1.93×10^{-9}	2.75	1.58×10^{-22}	2.35	7.58×10^{-25}	1.84	5.20×10^{-25}
350	3.21	3.49×10^{-6}	2.28	4.08×10^{-21}	1.99	4.11×10^{-23}	1.62	2.72×10^{-23}
400	2.69	9.62×10^{-4}	1.98	4.73×10^{-20}	1.76	8.47×10^{-22}	1.47	5.49×10^{-22}
450	2.33	7.58×10^{-2}	1.78	3.22×10^{-19}	1.60	9.18×10^{-21}	1.37	5.87×10^{-21}
500	2.08	2.49×10^{0}	1.63	1.52×10^{-18}	1.49	6.34×10^{-20}	1.30	4.02×10^{-20}
600	1.75	4.70×10^{2}	1.44	1.61×10^{-17}	1.34	1.23×10^{-18}	1.21	7.67×10^{-19}
700	1.55	1.99×10^{4}	1.32	9.18×10^{-17}	1.25	1.09×10^{-17}	1.15	6.74×10^{-18}
800	1.42	3.33×10^{5}	1.25	3.53×10^{-16}	1.19	5.88×10^{-17}	1.12	3.62×10^{-17}
900	1.33	3.00×10^{6}	1.19	1.05×10^{-15}	1.15	2.28×10^{-16}	1.09	1.40×10^{-16}
1000	1.27	1.74×10^{7}	1.16	2.58×10^{-15}	1.12	7.00×10^{-16}	1.08	4.25×10^{-16}
1500	1.12	3.58×10^{9}	1.07	5.09×10^{-14}	1.05	2.65×10^{-14}	1.03	1.56×10^{-14}
2000	1.07	5.30×10^{10}	1.04	2.95×10^{-13}	1.03	2.11×10^{-13}	1.02	1.21×10^{-13}
3000	1.03	8.09×10^{11}	1.02	2.43×10^{-12}	1.01	2.34×10^{-12}	1.01	1.30×10^{-12}

[a] Wigner tunneling correction factor κ_0 calculated for the imaginary frequency of the transition state TS1Br ($CBr_3OH^{\neq}$)

[b] Wigner tunneling correction factor κ_{HX} calculated for the imaginary frequency of the respective transition state TS2Br-HX $(CBr_3OH..HX)^{\neq}$

coefficients $k^{(2)}$ obtained from conventional transition state theory and $k^{(2)}_{exact}$ from Eq. (11) for CF_3OH+H_2O and CCl_3OH+H_2O reactions are, at temperatures below 1000 K, practically negligible, and even at 3000 K only slightly exceed 1% and 5% for CF_3OH and CCl_3OH, respectively. Therefore the conventional transition state theory is a useful tool in describing reaction kinetics, especially if one considers the precision of kinetic measurements.

Tables 4, 5, 6 also present the calculated values of the bimolecular rate coefficients, denoted by $k^{(2)}_{HX}$, for the CY_3OH+HX (X = F, Cl, and Br) reaction systems. The values of the second-order rate coefficients $k^{(2)}_{HX}$ are ordered similarly to the rate coefficients $k^{(1)}$ for the unimolecular dissociation of the perhalogenated alcohols. For the selected HX molecule, the fastest are reactions of CBr_3OH and the slowest those of CF_3OH. Analysis of the calculated rate coefficients indicates HF as the most effective accelerator. The presence of HF causes a decrease in the activation energy for the decomposition of CF_3OH by over 90 kJ mol^{-1}. For CCl_3OH and CBr_3OH, this reduction is lower, being 77 and 73 kJ mol^{-1}, respectively. The catalytic influence of HCl and HBr is distinctly weaker. However, both HCl and HBr result in lowering the energy barrier for the decomposition of CF_3OH, CCl_3OH, and CBr_3OH by 63-69 kJ mol^{-1}.

The lowest energy barrier in the CY_3OH+HX reaction systems of 59 kJ mol^{-1} occurs in the reaction of tribromomethanol with hydrogen fluoride. This results in the highest values of the rate coefficient for the reaction system CBr_3OH+HF, with $k^{(2)}$ of 1.6×10^{-22} $cm^3molecule^{-1}s^{-1}$ at 300 K. The highest value of the energy barrier of 94 kJ mol^{-1} is related with $CF_3OH+HCl$. This implies the considerably lower value of the second-order rate coefficient of 1.2×10^{-29} $cm^3molecule^{-1}s^{-1}$ at 300 K.

The differences in the heights of the energy barriers are reflected in the magnitudes of the calculated rate coefficients. For the bimolecular decomposition of CF_3OH, the largest one, i.e., 4.0×10^{-24} $cm^3molecule^{-1}s^{-1}$ at 300 K, is the rate coefficient $k^{(2)}$ for the CF_3OH+HF reaction system due to its having the lowest activation barrier. The energy barriers for the decomposition of CF_3OH in the presence of HCl and HBr are higher by over 25 kJ mol^{-1} compared with HF. Consequently, the rate coefficients $k^{(2)}_{HCl}$ and $k^{(2)}_{HBr}$ are a few orders of magnitude lower and close to one another, being 1.2×10^{-29} and 1.4×10^{-29} $cm^3molecule^{-1}s^{-1}$ at 300 K for the $CF_3OH+HCl$ and $CF_3OH+HBr$ reactions, respectively.

The rate coefficients for the bimolecular decay of CCl_3OH depend only slightly on the kind of hydrogen halide. The values of $k^{(2)}$ calculated at 300 K are 9.8×10^{-24}, 2.0×10^{-25}, and 1.1×10^{-25} $cm^3molecule^{-1}s^{-1}$ for CCl_3OH+HF, $CCl_3OH+HCl$, and $CCl_3OH+HBr$, respectively. The influence of the HX molecule on the decomposition of CBr_3OH distinctly depends on the type of hydrogen halide. The rate coefficient $k^{(2)}$ for CBr_3OH+HF is 1.6×10^{-22} $cm^3molecule^{-1}s^{-1}$ at 300 K. This is almost three orders of magnitude greater than the rate coefficients of 7.7×10^{-25} and 5.2×10^{-25} $cm^3molecule^{-1}s^{-1}$ for the $CBr_3OH+HCl$ and $CBr_3OH+HBr$ reactions, respectively. The temperature dependence of the rate coefficients for the

HX-catalyzed bimolecular decomposition of trifluoromethanol can be expressed in the form:

$$k^{(2)}(CF_3OH + HF) = 4.6 \times 10^{-14} \times (T/300)^{2.50} \times \exp(-6970/T) \ \ cm^3molecule^{-1}s^{-1} \quad (16)$$

$$k^{(2)}(CF_3OH + HCl) = 1.4 \times 10^{-14} \times (T/300)^{2.34} \times \exp(-10410/T) \ \ cm^3molecule^{-1}s^{-1} \quad (17)$$

$$k^{(2)}(CF_3OH + HBr) = 1.3 \times 10^{-14} \times (T/300)^{2.30} \times \exp(-10340/T) \ \ cm^3molecule^{-1}s^{-1} \quad (18)$$

Similar expressions also describe the bimolecular decomposition of trichloromethanol

$$k^{(2)}(CCl_3OH + HF) = 6.3 \times 10^{-14} \times (T/300)^{2.13} \times \exp(-6800/T) \ \ cm^3molecule^{-1}s^{-1} \quad (19)$$

$$k^{(2)}(CCl_3OH + HCl) = 8.1 \times 10^{-14} \times (T/300)^{2.72} \times \exp(-8025/T) \ \ cm^3molecule^{-1}s^{-1} \quad (20)$$

$$k^{(2)}(CCl_3OH + HBr) = 4.2 \times 10^{-14} \times (T/300)^{2.69} \times \exp(-6990/T) \ \ cm^3molecule^{-1}s^{-1} \quad (21)$$

and tribromomethanol

$$k^{(2)}(CBr_3OH + HF) = 8.2 \times 10^{-14} \times (T/300)^{2.28} \times \exp(-6045/T) \ \ cm^3molecule^{-1}s^{-1} \quad (22)$$

$$k^{(2)}(CBr_3OH + HCl) = 5.0 \times 10^{-14} \times (T/300)^{2.74} \times \exp(-7490/T) \ \ cm^3molecule^{-1}s^{-1}. \quad (23)$$

$$k^{(2)}(CBr_3OH + HBr) = 2.8 \times 10^{-14} \times (T/300)^{2.72} \times \exp(-7430/T) \ \ cm^3molecule^{-1}s^{-1} \quad (24)$$

The reaction rate at a given temperature is determined by either the magnitude of the rate coefficient or the concentrations of the reactants. The values of the activation barrier for the decomposition of CY_3OH in the presence of hydrogen halides are similar to that caused by the presence of water [29]. However, the concentration of water vapor in the atmosphere (10^{17} molecules cm^{-3} at altitudes below 5 km [1]) is incomparably greater than that of hydrogen halides. The presence of hydrogen halides may efficiently accelerate the decomposition of CY_3OH alcohol only when the concentration of HX is sufficiently high to satisfy the inequality $k_{HX}^{(2)}[HX] >> k^{(1)}$.Decay of the alcohol molecule CY_3OH leads to the formation of the respective hydrogen halide HY molecule. The decomposition of CY_3OH is always catalyzed by HY molecules, which are continuously formed in the reaction. However, depending on the concentration of HY, this autocatalytic effect can be positive or negative.

For an HF concentration lower than 10^{10} molecules cm^{-3} at room temperature, the rate of the bimolecular reaction CF_3OH+HF is less than that of the first-order decomposition of CF_3OH, and HF molecules may only inhibit the reaction rate as a result of binding reactants in the CF_3OH…HF molecular complex. The other hydrogen halides, HCl and HBr, can stimulate the decomposition of CF_3OH when they are present in the reaction area at sufficiently high concentrations. Genuine acceleration of the reaction rate requires a concentration of HCl and HBr higher than 3×10^{15} molecules cm^{-3} at 300 K. The levels of HCl in ambient air are not well established, but are probably in the low-ppb range (10^{10}-10^{11} molecules cm^{-3}) [1]. The atmospheric concentration of HBr is even smaller, on average a few ppt. This is clearly insufficient for promoting the removal of atmospheric CF_3OH, similarly as CCl_3OH and CBr_3OH.

Summary

The main aim of the present study is related to a theoretical analysis of the kinetics of the gas-phase decomposition of the perhalogenated methanols CF_3OH, CCl_3OH, and CBr_3OH. Theoretical investigations based on *ab initio* calculations of the reaction systems at the G2 level were performed to gain insight into the reaction mechanism. The results of the calculations also allow an estimation of the reaction energetics and the molecular properties of the structures taking part in the reaction.

The results of theoretical investigations show that the unimolecular dissociation of CF_3OH, CCl_3OH, and CBr_3OH proceeds with a high energy barrier. This implies low values of the rate coefficients for the reactions under investigations. Values of the high-pressure limiting rate coefficients $k_{diss,\infty}$ and their dependence on temperature for the thermal dissociation of CF_3OH, CCl_3OH, and CBr_3OH were derived using the conventional transition state theory in the temperature range 200-3000 K.

The kinetics and mechanism of the decomposition of the investigated alcohols in the presence of the hydrogen halides HF, HCl, and HBr were also analyzed theoretically. The calculated profiles of the potential energy surface of the reaction systems show that considerably lower energy pathways are accessible for the decomposition of CF_3OH, CCl_3OH, and CBr_3OH in presence of hydrogen halides. The mechanism of the reactions appears to be complex and consists of three consecutive elementary processes with the formation of pre- and post-reaction adducts. The thermal stability of these molecular complexes is determined by the strength of the respective hydrogen bonds formed during reactions. In consequence, the binding energy of the formed adducts increases in agreement with the strength of the formed H…X bonds, H…Br < H…Cl < H…F.

The presence of hydrogen halides distinctly decreases the energy barrier for the bimolecular decomposition of the alcohols CF_3OH, CCl_3OH, and CBr_3OH. Therefore the HX-accelerated bimolecular decomposition of the halogenated alcohols may proceed very rapidly if the concentration of the hydrogen halide in the reaction system is sufficiently high. However, the atmospheric concentrations of the hydrogen halides are small. Consequently, the reactions $CF_3OH/CCl_3OH/CBr_3OH$+HX are of no importance under typical atmospheric conditions.

The investigated reactions $CF_3OH/CCl_3OH/CBr_3OH$+HX may, however, acquire significance in the kinetic modeling of the complex reaction systems studied on a laboratory scale, especially in the case of reactions which proceed with the formation of the perhalogenated alcohols CF_3OH, CCl_3OH, and CBr_3OH in the presence of sizable concentrations of the halogen halides. Under these conditions, the rate of decay of the perhalogenated methanols may strongly depend on the concentrations of hydrogen halides. The values of the rate coefficients calculated in this study allow a description of the kinetics of the reactions under investigation in a wide temperature range. They should be useful in the kinetic analysis and modeling of such reaction systems.

Acknowledgments This research was supported by Wroclaw Medical University under grant no. ST-263. The Wroclaw Center of Networking and Supercomputing is acknowledged for the generous allotment of computer time.

References

1. Finnlayson-Pitts BJ, Pitts JN (2000) Chemistry of the Upper and Lower Atmosphere. Academic, San Diego
2. Wayne RP, Poulet G, Biggs P, Burrows JP, Cox RA, Crutzen PJ, Hayman GD, Jenkin ME, LeBras G, Moortgat GK, Platt U, Schindler RN (1995) Atmos Environ 29:2677–2881
3. Wallington TJ, Dagaut P, Kurylo MJ (1992) Chem Rev 92:667–710
4. Sehested J, Wallington TJ (1993) Environ Sci Technol 27:146–152
5. Wallington TJ, Schneider WF (1994) Environ Sci Technol 28:1198–1200
6. Schneider WF, Wallington TJ, Minschwaner K, Stahlberg EA (1995) Environ Sci Technol 29:247–250
7. Huey LG, Hanson DR, Lovejoy ER (1995) J Geophys Res 100:18771–18774
8. Bednarek G, Kohlmann JP, Saathoff H (1995) Zellner R. Z Phys Chem Munich 188:1–15
9. Lovejoy ER, Huey LG, Hanson DR (1995) J Geophys Res 100:18775–18780
10. Wallington TJ, Hurley MD, Schneider WF, Sehested J, Nielsen OJ (1993) J Phys Chem 97:7606–7611
11. Francisco JS (1991) Chem Phys 150:19–27
12. Bock CW, Trachtman M, Niki H, Mains GJ (1994) J Phys Chem 98:7976–7980
13. Francisco JS (1994) Chem Phys Lett 218:401–405
14. Schneider WF, Wallington TJ, Huie RE (1996) J Phys Chem 100:6097–6103
15. Kim SJ, Song HS (1999) Bull Korean Chem Soc 20:1493–1500
16. Brudnik K, Jodkowski JT, Ratajczak E, Venkatraman R, Nowek A, Sullivan RH (2001) Chem Phys Lett 345:435–444
17. Brudnik K, Jodkowski JT, Ratajczak E (2003) J Mol Struct 656:333–339
18. Brudnik K, Jodkowski JT, Ratajczak E (2003) Bull Pol Acad Sci Chem 51:77–91
19. Fernández LE, Varetti EL (2003) J Mol Struct THEOCHEM 629:175–183
20. Tyndall GS, Wallington TJ, Hurley MD, Schneider WF (1993) J Phys Chem 97:1576–1582
21. Wallington TJ, Schneider WF, Barnes I, Becker KH, Sehested J, Nielsen OJ (2000) Chem Phys Lett 322:97–102
22. Schnell M, Mühlhäuser M, Peyerimhoff SD (2002) Chem Phys Lett 361:1–7
23. Sun H, Bozzelli JW (2001) J Phys Chem A 105:4504–4516
24. Brudnik K, Jodkowski JT, Nowek A, Leszczynski J (2007) Chem Phys Lett 435:194–200
25. Montgomery JA, Michels HH, Francisco JS (1994) Chem Phys Lett 220:391–396
26. Notario R, Castaño O, Abboud JLM (1996) Chem Phys Lett 263:367–370
27. Espinosa-Garcia J (1999) Chem Phys Lett 315:239–247
28. Segovia M, Ventura ON (1997) Chem Phys Lett 277:490–496
29. Brudnik K, Wójcik-Pastuszka D, Jodkowski JT, Leszczynski J (2008) J Mol Model 14:1159–1172
30. Vöhringer-Martinez E, Hansmann B, Hernandez H, Francisco JS, Troe J, Abel B (2007) Science 315:497–501
31. Garrett BC (2004) Science 303:1146–1147
32. Takahashi K, Kramer ZC, Vaida V, Skodje RT (2007) Phys Chem Chem Phys 9:3864–3871
33. Curtiss LA, Raghavachari K, Trucks GW, Pople JA (1991) J Chem Phys 94:7221–7230
34. Frisch MJ, Trucks GW, Schlegel HB, Scuseria GE, Robb MA, Cheeseman JR, Montgomery JA, Vreven T, Kudin KN, Burant JC, Millam JM, Iyengar SS, Tomasi J, Barone V, Mennucci B, Cossi M, Scalmani G, Rega N, Petersson GA, Nakatsuji H, Hada M, Ehara M, Toyota K, Fukuda R, Hasegawa J, Ishida M, Nakajima T, Honda Y,

Kitao O, Nakai H, Klene M, Li X, Knox JE, Hratchian HP, Cross J B, Adamo C, Jaramillo J, Gomperts R, Stratmann RE, Yazyev O, Austin AJ, Cammi R, Pomelli C, Ochterski JW, Ayala PY, Morokuma K, Voth GA, Salvador P, Dannenberg JJ, Zakrzewski VG, Dapprich S, Daniels AD, Strain MC, Farkas O, Malick DK, Rabuck AD, Raghavachari K, Foresman JB, Ortiz JV, Cui Q, Baboul AG, Clifford S, Cioslowski J, Stefanov BB, Liu G, Liashenko A, Piskorz P, Komaromi I, Martin RL, Fox DJ, Keith T, Al-Laham MA, Peng CY, Nanayakkara A, Challacombe M, Gill PM W, Johnson B, Chen W, Wong MW, Gonzalez C, Pople JA (2003) Gaussian 03, Revision B.03. Gaussian Inc, Pittsburgh PA

35. Johnston HS (1966) Gas-Phase Reaction Rate Theory. Ronald, New York
36. Laidler KJ (1969) Theories of Chemical Reaction Rates. McGraw-Hill, New York
37. Burk P, Koppel IA, Rummel A, Trumlar A (2000) J Phys Chem A 104:1602–1607
38. Mozurkevich M, Benson SW (1984) J Phys Chem 88:6429–6435
39. Chen Y, Rauk A, Tschuikow-Roux E (1991) J Phys Chem 95:9900–9908
40. Jodkowski JT, Rayez MT, Rayez JC, Bérces T, Dóbé S (1998) J Phys Chem A 102:9219–9229
41. Jodkowski JT, Rayez MT, Rayez JC, Bérces T, Dóbé S (1998) J Phys Chem A 102:9230–9243
42. Jodkowski JT, Rayez MT, Rayez JC, Bérces T, Dóbé S (1999) J Phys Chem A 103:3750–3765